Cortical blood flow assessment with frequency-domain laser Doppler microscopy

Michael Atlan
Benoît C. Forget
Albert C. Boccara
Université Pierre et Marie Curie
Ecole Supérieure de Physique et de Chimie
Industrielles de la Ville de Paris
Laboratoire d'Optique
CNRS UPR A0005
10 rue Vauquelin
F-75231 Paris cedex 05
France
E-mail: atlan@optique.espci.fr

Tania Vitalis
Armelle Rancillac
École Supérieure de Physique et de Chimie
Industrielles de la Ville de Paris
Laboratoire de Neurobiologie et Diversité Cellulaire
CNRS UMR 7637
10 rue Vauquelin
F-75231 Paris cedex 05
France

Andrew K. Dunn
University of Texas at Austin
Biomedical Engineering Department
1 University Station, CO800
Austin, Texas 78712-0238

Michel Gross
Ecole Normale Supérieure
Laboratoire Kastler-Brossel
UMR 8552 (ENS, CNRS, UMPC)
10 rue Lhomond
F-75231 Paris cedex 05
France

Abstract. We report the assessment of cerebral blood flow (CBF) changes with a wide-field laser Doppler imager based on a CCD camera detection scheme, *in vivo*, in mice. The setup enables the acquisition of data in minimally invasive conditions. In contrast with conventional laser Doppler velocimeters and imagers, the Doppler signature of moving scatterers is measured in the frequency domain, by detuning a heterodyne optical detection. The quadratic mean of the measured frequency shift is used as an indicator of CBF. We observe a significant variability of this indicator in an experiment designed to induce blood flow changes. *© 2007 Society of Photo-Optical Instrumentation Engineers.* [DOI: 10.1117/1.2715184]

Keywords: laser Doppler velocimetry; coherent optical systems; holography applications; heterodyning; interferometry; lasers in medicine.

Paper 06173R received Jul. 13, 2006; revised manuscript received Oct. 12, 2006; accepted for publication Nov. 28, 2006; published online Apr. 26, 2007.

1 Introduction

In vivo imaging is necessary in a wide range of biomedical applications. In the brain, neurovascular coupling has been widely studied due to its importance in developing a better understanding of both the normal and diseased brain. The hemodynamic component to the neurovascular response consists of the changes in cerebral blood flow (CBF), blood volume, and hemoglobin concentration. To fully understand the neurovascular coupling, it is desirable to image all of the components of the hemodynamic response simultaneously. Optical methods have been widely used to image hemodynamic changes in the cortex, however, most of the optical methods have been limited to imaging only the changes in blood volume or hemoglobin concentration. The primary limitation of full-field imaging of CBF changes has been the lack of a method with the necessary temporal and spatial resolutions. Only recently has full-field imaging of all hemodynamic components been demonstrated in studies of neurovascular coupling.[1,2] Therefore, it is essential to develop improved techniques for imaging blood flow. A light-based apparatus can be minimally to noninvasive, and easy to design. Two main classes of techniques for detecting CBF have emerged: laser Doppler velocimetry (LDV) and speckle contrast analysis (SCA). Both rely on the interferometric properties of coherent light. SCA techniques are based on the measurement of the local spatial blur rate of the intensity of speckle pattern present on the images. Based on a time-domain measurement, LDV techniques reveal the frequency distribution of Doppler-broadened light. It was shown that LDV and SCA were two distinct approaches to assess the same underlying phenomenon: dynamic light scattering.[3–6]

Address all correspondence to Michael Atlan, labo. d'optique, espci, 10 rue vauquelin Paris, France 75005 France; Tel: +33144323418; Fax: +33144323434; E-mail: atlan@optique.espci.fr

1083-3668/2007/12(2)/024019/8/$25.00 © 2007 SPIE

Stern et al. designed the landmark laser Doppler instrument for bioflow assessment.[7] The first attempt to use the spatial properties of dynamic speckle patterns for flow visualization were reported by Fercher and Briers,[8] whose work led to the development of laser SCA imaging techniques.[9–11] Both techniques have shown a great potential in CBF assessment *in vivo*. LDV has become popular[12–14] for focal measurements of dynamic changes of CBF, while SCA is rapidly becoming a common tool for imaging purposes.[15,16] The advantage of SCA is a high temporal resolution in conjunction with a good spatial resolution. Its major weakness lies in the fact that the speckle contrast values are not linearly related to blood flow velocity,[15] although relative CBF images can be calculated from speckle contrast images by assuming a particular form for the underlying velocity distribution. On the other hand, LDV yields quantitative information (spectra), but its drawback is the limited performance of scanning systems in terms of spatial and temporal resolution. Postprocessing of the laser Doppler spectra[17,18] can enhance the detection capabilities and resolving power of LDV instruments, in particular, for low flows and vascular differentiation, but cannot improve temporal resolution.

The laser Doppler flowmetry signal was reported[19] to be correlated to actual blood flow *in vivo*, but with significant variability from point-to-point measurements within an area of a tissue, which clearly pointed out the necessity for laser Doppler imaging (LDI) techniques. Standard scanning laser Doppler instruments,[20] based on time-domain measurements, provide spatial resolution at the expense of temporal resolution. A time-domain laser Doppler measurement technique with a fast CMOS camera was introduced[21,22] as well as new methods to take advantage of the time-domain integration of cameras,[23,24] providing alternatives to speckle contrast analysis to perform wide-field imaging of bioflow.

We reported a CBF assessment in mice with a wide-field LDI instrument,[26] relying on a frequency-domain detection of scattered light,[25] which is an alternative to either time-domain or spatial-domain detection techniques.[6] In this scheme, scattered light is analyzed by a detuned local oscillator (LO), which consists of a fraction of the main laser beam shifted in frequency, and detected by a CCD camera, acting as a narrow spectral filter, enabling one to scan the spectral content of the object field. The main strength of this tool lies in the spatial resolution of the Doppler maps, which is suitable for functional brain imaging since the lack of spatial resolution has been noted to be a limitation of conventional LDI. Here, we report the results of experiments designed to determine whether the instrument would enable detection of subtle changes of CBF in mice.

2 Description of the Instrument

2.1 *Experimental Setup*

The basic principles of the instrument were described previously.[26] However, we provide a summary of the experimental setup here for clarity. The apparatus is designed to analyze scattered light in the frequency domain. The object is illuminated by the main laser beam, whose field E_L undergoes dynamic scattering. The scattered (or object) field E_O carries the signature of the local dynamic state of the object within its

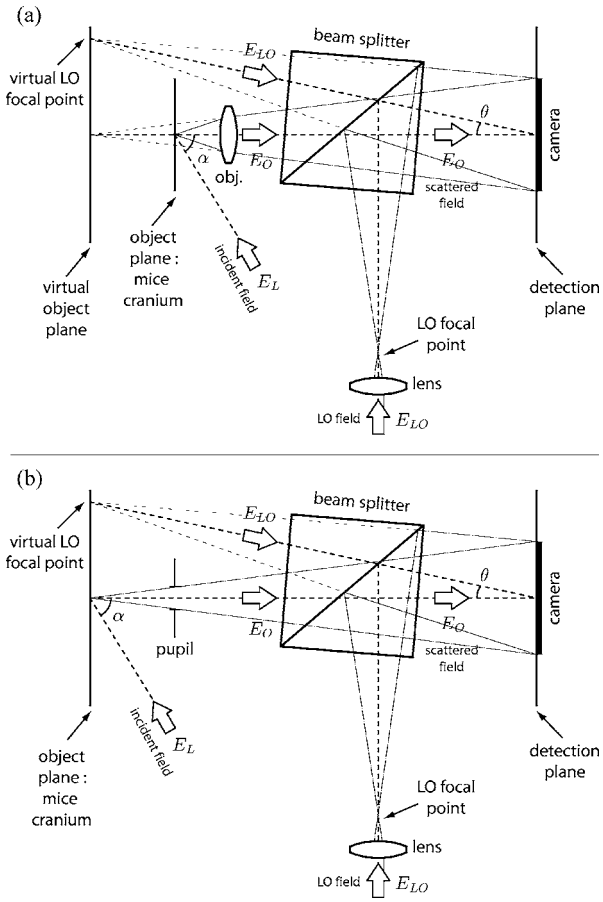

Fig. 1 Optical configuration (the whole apparatus is described in Ref. 26). The field E_L shines the mouse cranium whose skin was excised, with an average incidence angle α. The object (scattered) field E_O and reference field E_{LO} propagation axes make a θ angle. (a) An ×4 microscope objective (obj.) is used to reduce the field of view and (b) configuration without objective in the object arm. A pupil prevents parasitic light to be recorded by the camera.

spectrum. Early studies[27] of Doppler broadening of light by flows showed that the Doppler shift for one scattering event is

$$\omega_D = (\mathbf{k}_s - \mathbf{k}_i)\mathbf{v}, \tag{1}$$

where $\mathbf{k}_i$ is the incident wave vector, $\mathbf{k}_s$ is the scattered wave vector, and $\mathbf{v}$ is the instantaneous particle velocity. Further work showed that the distribution of scatterer velocities is linked to the frequency distribution of probing light.[4] To measure a spatially resolved spectrum onto the object, E_O is mixed with a detuned LO field E_{LO} on an array detector.[26]

In the experimental setup, the object (a mouse cranium) was illuminated over the region to be imaged with an average incidence angle $\alpha \approx 60$ deg. The scattered field E_O was mixed with a frequency-shifted LO field E_{LO}, split off from the main laser beam. To achieve sensitive detection, a spatiotemporal heterodyning of the scattered field was performed. The optical configuration is based either on a classic off-axis lensless Fourier holography scheme[28] [sketched in Fig. 1(b)] or a slightly modified one, into which a microscope objective (Olympus, ×4 magnification) took place in the object arm [Fig. 1(a)]. The choice of the presence of a microscope objective in the

apparatus is dictated by spatial resolution demand. A single-mode 80-mW cw Mitsubishi ML120G21 diode provided the main laser beam at 658 nm (angular frequency ω_L). Two Bragg cells (acousto-optic modulators, AOMs), were used to shift the LO frequency by the tunable difference $\Delta\omega_{\mathrm{AOM}}$ of their (coherent) driving frequencies: $\omega_{\mathrm{LO}}=\omega_L+\Delta\omega_{\mathrm{AOM}}$. The LO beam was focused by a 1-cm-focal-length lens, to place the virtual LO focal point in the object plane (Fig. 1). A beam-splitter was used to combine E_O and E_{LO} with a small off-axis angle $\theta\approx 1$ deg. The distance between the detection plane and the object plane (or virtual object plane) was 50 cm. A 1.3-megapixel PCO PixelFly camera [frame rate $\omega_S/(2\pi)=8$ Hz, square pixels, pixel size 6.7 μm] was used to record a sequence of m images $\{I_k\}$, where $k=1,\ldots,m$. For each detuning frequency of interest, the camera sampled a modulated interference pattern. This modulation is a consequence of optical mixing of the object field with the detuned LO field.

2.2 *Data Acquisition*

A digital hologram was recorded according to the frequency-shifting method introduced in the heterodyne holography technique, used in several imaging and detection schemes[29–31] and that turns out to be sensitive enough to discriminate Doppler-shifted photons among heavily scattered light[29,31] according to their frequency. The frequency-shifting method was chosen for its accuracy.[32]

The LO frequency was set to $\omega_{\mathrm{LO}}=\omega_L+\Delta\omega+\omega_S/n$, where $n=4$, to sample a map of the $\Delta\omega$ angular frequency component [corresponding to the $\Delta f=\Delta\omega/(2\pi)$ frequency, in hertz] of the scattered field E_O impinging on the camera.[25] The choice of $n=4$ meant that four images were used to measure both quadratures of the scattered field. A sequence of $m=32$ images was recorded at each detuning frequency for averaging purposes to improve the signal-to-noise ratio (SNR). Each spatial map at a given temporal frequency point was measured in $4\times 1/8=0.5$ s and averaged over $32\times 1/8=4$ s.

2.3 *Signal Demodulation*

The power $S(\Delta\omega)$ of the $\omega_L+\Delta\omega$ frequency component of the measured object field E_O was computed onto the pixels of the image, according to the n-phase demodulation method.[29,30,32] It is calculated as

$$S(\Delta\omega)=A\left|\sum_{k=1}^{n} I_k \exp[-2i(k-1)\pi/n]\right|^2, \qquad (2)$$

where A is a constant, and $i^2=-1$. Two-dimensional maps of $S(\Delta\omega)$ were realized for each arbitrary frequency point $\Delta\omega$, one at a time, set by the detuning frequency of the LO.

2.4 *Image Reconstruction*

Two similar optical configurations were used. One is a modified lensless Fourier holographic setup, into which a $4\times$ magnification microscope objective was placed in the object arm [as sketched in Fig. 1(a)]. The other is a regular lensless Fourier setup [Fig. 1(b)]. In both cases, the LO focal point was positioned in the relevant object plane to cause the E_O and E_{LO} average curvatures to match in the detection plane. The presence of the microscope objective in the setup was guided by the desired spatial extent of the image. The field of view was $\sim 8\times 12$ mm without and $\sim 2\times 3$ mm with the $4\times$ objective.

The lensless Fourier setup was used to avoid the necessity for a general Fresnel reconstruction algorithm[33] to assess the spatial distribution of the scattered field in the object plane. In this case, the reconstruction algorithm consisted of one spatial fast Fourier transform[34] (FFT).

2.5 *Postprocessing*

A logarithmic-scale quantity S_{dB} was formed to display spectral maps

$$S_{\mathrm{dB}}(\Delta\omega)=10\log_{10}\left[\frac{S(\Delta\omega)}{N(\Delta\omega)}\right], \qquad (3)$$

where $N(\Delta\omega)$ is the quantity $S(\Delta\omega)$ assessed in a region of the reconstructed hologram where the object light contribution is null. It was reported to be shot-noise dominated.[31]

To assess bioflow,[7,35] the quadratic mean (or root mean square, rms) of the frequency shift is calculated as

$$\langle\Delta\omega^2\rangle^{1/2}=\left[\frac{\sum S(\Delta\omega_k)\Delta\omega_k^2}{\sum S(\Delta\omega_k)}\right]^{1/2}, \qquad (4)$$

where the sums are made over 80 linearly spaced points of measurement $\Delta\omega_k$ between 0 and 2528 Hz (the spacing interval is 32 Hz).

To increase the SNR, a sequence of $m=32$ images was taken to build each $S(\Delta\omega)$ map at one given $\Delta\omega$ frequency point, setting $\Delta\omega_{\mathrm{AOM}}=\Delta\omega+\omega_S/n$, where $n=4$. Note that $S(\Delta\omega)$ was averaged over the m-image sequence. Each frequency point of the spatial distribution $S(\Delta\omega)$ was measured in $32\times 1/8=4$ s. The measurement of a whole cube of data (space, frequency) took 5 min and 20 s (=32 images $\times 80$ frequency shifts $\times 1/8$ s exposure time).

3 Experiments

The results of three different experiments are presented: post-mortem residual flow mapping (detection of reduced blood flow), minimally invasive CBF detection *in vivo*, and monitoring of drug-induced CBF changes through the intact cranium.

Animal procedures were conducted in strict compliance with approved institutional protocols and in accordance with the provisions for animal care and use described in the European Communities Council directive of November 24, 1986 (86-16-09/EEC). In total, five C57/Bl6 mice (Charles River) aged P25 to P30 were used. Anesthesia was achieved by injecting a mixture of xylazine [1 mg/kg intraperitoneal (IP)] and ketamine (10 mg/kg IP). Cranial skin and subcutaneous tissues were excised linearly over the sagittal suture. Animals were positioned on a stereotaxic frame (World Precision Instruments) to ensure stability of the preparation. Cortical bones were regularly hydrated with a saline solution to prevent them from drying.

A first set of data was obtained from three control animals, which were used to determine the optimal setup configuration, to determine the sensitivity of our technique and to visualize

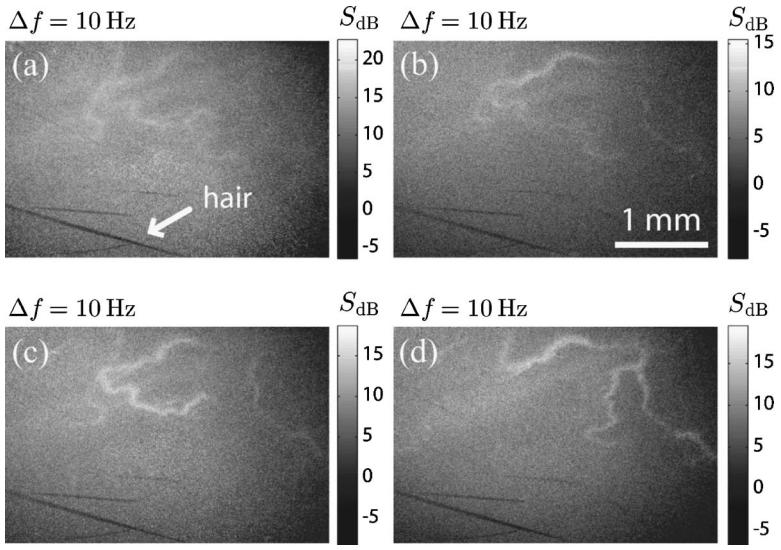

Fig. 2 Dimensionless S_{dB} maps with Δf=10 Hz of measurements in dead mice (test animals), with the optical configuration sketched in Fig. 1(a) obtained (a) ~10 min after death and (b), (c), and (d) at 1-min consecutive intervals. Images were made in a 5-×5-mm cranial window carved out from the skull. The colorbar is scaled to the amplitude of the recorded signal.

intact superficial blood vessels and extract Doppler information. Throughout this procedure, a microscope objective was used in the object arm, as represented in Fig. 1(a). The resulting imaging field of view is ~2×3 mm.

3.1 *Detection of Reduced Blood Flow*

The laser Doppler technique is a useful complement to other noninvasive methods, especially clinical assessment, in the determination of brain death in the newborn. Brain death is characterized by well-defined sequences in deterioration of the flow velocity waveform in blood vessels. This sequence was previously shown to consist of a loss of diastolic flow, appearance of retrograde flow during diastole, diminution in systolic flow in the anterior cerebral artery, and ultimately, lack of flow in the anterior cerebral artery.[36] These modifications are the results of a progressive increase in cerebrovascular resistance and a progressive decrease in cerebral perfusion, compatible with the diffuse cerebral necrosis and oedema documented postmortem. Our first set of experiments aimed to determine the threshold of sensitivity of our apparatus. We sought to determine whether our apparatus would detect the Doppler signature of the remaining perfusion in a dead animal. The animal was deeply anesthetized using an overdose of the xylazine-ketamine mixture. A cranial window (excision of a small part of the skull) was performed and images of CBF were collected more than 10 min after cessation of visible heart-beating. Figures 2(a)–2(d) represent S_{dB} maps at the Doppler shift Δf=10 Hz, taken at 1-min intervals, and possibly suggest a residual capillary flow. Those images are consistent with the presence of a residual flow in the brain persisting soon after death, although the exact origin of this observed Doppler signal is not known.

3.2 *Minimally Invasive Assessment of Cerebral Blood Flow*

Images of the brains of two mice were done through their intact skulls (measured thickness of 0.27 mm medial and 0.22 mm lateral), without altering it. A sequence of S_{dB} maps at different frequency shifts is reported in Figs. 3(a)–3(f). Each of the maps represented in Fig. 3 was obtained in the same mouse in a measurement time of 4 s [from 32 images recorded at $\omega_S/(2\pi)$=8 Hz]. The most striking result is the contrast reversal between the vessels and the parenchyma regions in the map at Δf=0 Hz [Fig. 3(a)] and the map at Δf =384 Hz [Fig. 3(c)]. A more subtle difference can be observed between Figs. 3(c) and 3(d), corresponding to the 384- and 512-Hz Doppler shifts. The flow in the right arm of the central Y-shaped vessel (arrow) has a weak contribution at the 512 Hz, suggesting a lower CBF through it than through its left counterpart. An even more subtle effect can be seen in Fig. 3(e): One can distinguish the presence of a transversal vessel (arrows), which cannot be perceived below 1 kHz, suggesting it has a high CBF. Those preliminary results attest to a sensitivity and dynamic range suitable for CBF studies. The typical response frequencies of the flow in the Y-shaped vessels in Figs. 3(c) and 3(d) are in the 400- to 500-Hz range, whereas in Fig. 2, we see this signal for a 10-Hz frequency shift, which demonstrates the ability of the setup to map the Doppler signature of very small flows. As an indication, if we make the assumption that the collected light undergoes one scattering event and only in-plane velocities participate in the Doppler shift of light, then, according to Eq. (1), the order of magnitude of the velocity corresponding to a Doppler signal at 10 Hz, mapped in Fig. 2, would be ~10 μm s^{-1}.

3.3 *Real-Time Assessment of Drug Effects*

We tested whether our setup would enable detection of small and reversible variations of CBF under minimally invasive conditions. Therefore, we used a pharmacological paradigm well known to induce modification of blood flow. Effects of variation in monoamine levels (NE, 5-HT) on blood flow are well studied. We thought to monitor the modifications in CBF occurring after a single IP injection with pargyline (100 mg/kg/IP, single injection). Pargyline is an inhibitor of

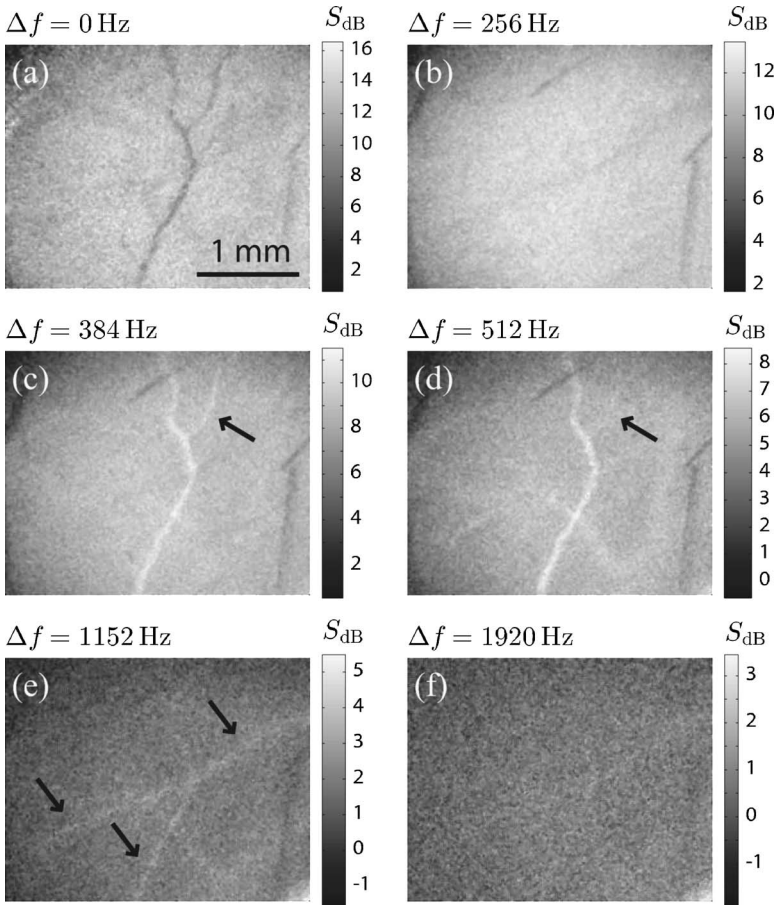

Fig. 3 Dimensionless S_{dB} of maps of *in vivo* measurement with an intact skull and the skin removed for several Δf frequency components. The optical configuration is sketched in Fig. 1(a). The colorbar is scaled to the amplitude of the recorded signal, for each frequency point.

monoamine oxidase (I-MAO) type A and type B (MAOA; MAOB), which are two membrane-bound mitochondrial flavoproteines that oxidatively deaminate a broad range of biogenic amines, including monoaminergic neurotransmitters serotonin and catecholamines[37] (dopamine, norepinephrine, and adrenaline). In rodents, as in many other species, cerebral blood vessels display aminergic innervations and MAO activities.[38,39] I-MAOs are largely used and known to produce a fast increase in brain serotonin and norepinephrine levels within 5 to 60 min after a single intraperitoneal injection[40–42] and are known to increase blood vessel pressure within minutes *in vivo*.[42]

In this set of experiments we chose to increase the field of view of the control procedure. To make the image area match the whole cranium of the mouse ($\sim 1 \times 1$ cm), the microscope objective is removed from the setup to benefit from the natural heterodyne image field.[43] In our experiment, data were collected in the same animal from the instant of drug injection and every 10 min after the injection over a period of 1 h 20 min. An average rms Doppler shift map is shown in Fig. 4(a), into which 16 regions of interest (ROIs) are defined. ROIs 1.x and 3.x correspond to vessels, ROIs 2.x to midline, and ROIs 4.x are in the parenchyma. We observed a decrease in CBF occurring between 10 and 20 min after the injection that mostly affects small-caliber blood vessels [10 to 20% decrease in rms Doppler shift see Figs. 4(c)–4(f)]. At 1 h 20 min after pargyline injection, CBF had reached preinjection values. The most important relative CBF variation appears to occur in the parenchyma and the vessel ROIs. As an indication under the previously cited assumption, the order of magnitude of the rms velocity corresponding to a 1000-Hz rms Doppler shift is ~ 1 mm s^{-1}.

Our study is consistent with previous ones showing that blood vessel contractions are in part induced by activation of catecholaminergic and serotoninergic receptors. *In vivo* and *in vitro*, catecholamines have been shown to produce responses that are consistent with vasoconstriction (contraction, isometric tension, increase in perfusion pressure, and decrease in flow).[45,46] Serotonin has more complex effects on the cardiovascular system but is generally contractile in its effects,[47,48] except for meningal blood vessels.[49] Serotonin may act on S2-serotonergic receptors located on vascular smooth muscles and has also been described to act indirectly by amplifying the response to norepinephrine[50,51] and other agonists, of releasing constrictor substance(s) from the endothelium. In addition, the increase in heart rate elicited by monoamine elevation may partially account for an increase in blood pressure. The design of our study does not enable discrimination of whether the observed changes are the result of elevations of 5-HT and/or catecholamines, or whether changes in CBF are due to an increase in heart rate, but this was beyond the scope of our study.

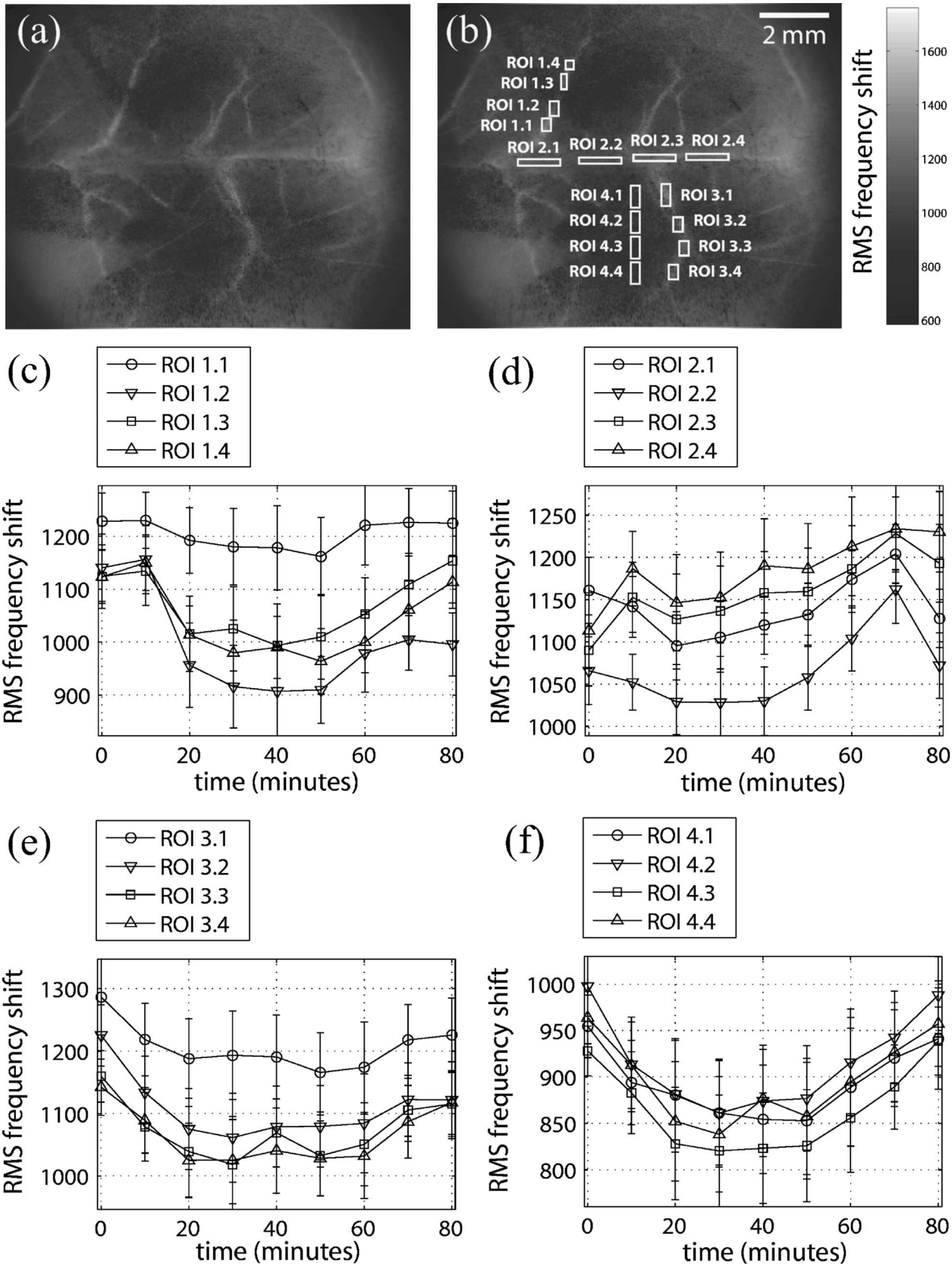

Fig. 4 Mouse cranium from which the skin and subcutaneous tissue were excised observed in the retrodiffusion configuration [Fig. 1(b)]: (a) map of the rms Doppler frequency shift of light (in hertz), (b) replication of (a) intendeol to display the chosen ROIs for the calculus of the rms Doppler shift. *In vivo* measurement of the intact skull. The dorsal view of the mouse cranium shows the superficial dorsal venous system (transverse and sigmoid sinus and the retroglenoid veins) and some of the superficial cerebral arteries. The rostral part of the brain is to the left.[44] (c) to (f): plots of the rms Doppler frequency shift of light averaged in ROIs outlined in (b).

4 Conclusion

The scope of this study was to report monitoring and mapping of drug-induced average blood flow changes in mice brains, in minimally invasive conditions. As an indicator of flow, we used the rms Doppler shift calculated with 80 linearly spaced spectral points between 0 and 2.5 kHz. Because the whole spectrum measurement lasted several minutes, this indicator is a time-averaged value of the Doppler signature of the actual flow.

Our setup was based on a camera detection used to measure a map of one spectral component of the scattered light out of a few recorded images. Both quadratures of the scattered field carrying the Doppler information where measured in the detector plane and propagated numerical to the object plane, to produce a tunable spectral image. The heterodyne off-axis configuration enables sensitivity suitable for *in vivo* Doppler mapping of CBF. Our study demonstrated that the frequency-domain wide-field laser Doppler imager is able to detect subtle changes in the CBF of a mouse. We report the suitability of the presented scheme to efficiently measure the spectral signature of a wide range of blood flows, beyond the detector bandwidth.

Our results show a significant spatial discrepancy of the signal, justifying the necessity of the proposed high-spatial-resolution functional imager. To enable a high temporal resolution, fewer spectral points might be recorded to increase the sampling rate, and indicators other than the rms Doppler shift used here to assess flow might be used with this instrument.

Acknowledgments

The authors are thankful to the reviewers of this paper who have contributed to making it clearer. We acknowledge support from Paris VI University (BQR grant).

References

1. C. Ayata, A. K. Dunn, Y. Gursoy-Ozdemir, Z. Huang, D. A. Boas, and M. A. Moskowitz, "Laser speckle flowmetry for the study of cerebrovascular physiology in normal and ischemic mouse cortex," *J. Cereb. Blood Flow Metab.* **24**(7), 744–755 (2004).
2. A. K. Dunn, A. Devor, A. M. Dale, and D. A. Boas, "Spatial extent of oxygen metabolism and hemodynamic changes during functional activation of the rat somatosensory cortex," *Neuroimage* **27**(2), 279 (2005).
3. B. J. Berne and R. Pecora, *Dynamic Light Scattering*, Wiley, New York (1976).
4. R. Bonner and R. Nossal, "Model for laser Doppler measurements of blood flow in tissue," *Appl. Opt.* **20**, 2097–2107 (1981).
5. T. Yoshimura, "Statistical properties of dynamic speckles," *J. Opt. Soc. Am. A* **3**, 1032–1054 (1986).
6. J. D. Briers, "Laser Doppler and time-varying speckle: a reconciliation," *J. Opt. Soc. Am. A* **13**, 345–350 (1996).
7. M. D. Stern, D. L. Lappe, P. D. Bowen, J. E. Chimosky, G. A. Holloway, H. R. Keiser, and R. L. Bowman, "Continuous measurement of tissue blood flow by laser-Doppler spectroscopy," *Am. J. Physiol.* **232**(4), H441–H448 (1977).
8. A. F. Fercher and J. D. Briers, "Flow visualisation by means of single-exposure speckle photography," *Opt. Commun.* **37**, 326–330 (1981).
9. J. A. Briers and S. Webster, "Quasi real-time digital version of single-exposure speckle photography for full-field monitoring of velocity or flow fields," *Opt. Commun.* **116**, 36-42 (1995).
10. J. D. Briers and S. Webster, "Laser speckle contrast analysis (LASCA): a nonscanning, full-field technique for monitoring capillary blood flow," *J. Biomed. Opt.* **1**(2), 174–179 (1996).
11. J. D. Briers, G. Richards, and X. W. He, "Capillary blood flow monitoring using laser speckle contrast analysis (LASCA)," *J. Biomed. Opt.* **4**(1), 164–175 (1999).
12. R. L. Haberl, M. L. Heizer, A. Marmarou, and E. F. Ellis, "Laser-Doppler assessment of brain microcirculation: effect of systemic alterations," *Am. J. Physiol. Heart Circ. Physiol.* **256**, H1247–H1254 (1989).
13. M. Fabricius and M. Lauritzen, "Laser-Doppler evaluation of rat brain microcirculation: comparison with the [14c]-iodoantipyrine method suggests discordance during cerebral blood flow increases," *J. Cereb. Blood Flow Metab.* **16**(1), 156–161 (1996).
14. D. Malonek, U. Dirnagl, U. Lindauer, K. Yamada, I. Kanno, and A. Grinvald, "Vascular imprints of neuronal activity: relationships between the dynamics of cortical blood flow, oxygenation, and volume changes following sensory stimulation," *Proc. Natl. Acad. Sci. U.S.A.* **94**, 14826–14831 (1997).
15. A. Dunn, H. Bolay, M. A. Moskowitz, and D. A. Boas, "Dynamic imaging of cerebral blood flow using laser speckle," *J. Cereb. Blood Flow Metab.* **21**(3), 195–201 (2001).
16. H. Bolay, U. Reuter, A. K. Dunn, Z. Huang, D. A. Boas, and M. A. Moskowitz, "Intrinsic brain activity triggers trigeminal meningeal afferents in a migraine model," *Nat. Med.* **8**, 136–142 (2002).
17. M. L. Arildsson, K. Wardell, and G. E. Nilsson, "Higher order moment processing of laser Doppler perfusion signals," *J. Biomed. Opt.* **2**(4), 358–363 (1997).
18. M. Larsson and T. Stromberg, "Toward a velocity-resolved microvascular blood flow measure by decomposition of the laser Doppler spectrum," *J. Biomed. Opt.* **11**(1), 014024 (2006).
19. G. J. Smits, R. J. Roman, and J. H. Lombard, "Evaluation of laser-Doppler flowmetry as a measure of tissue blood flow," *J. Appl. Physiol.* **61**(2), 666–672 (1986).
20. T. J. H. Essex and P. O. Byrne, "A laser Doppler scanner for imaging blood flow in skin," *J. Biomed. Eng.* **13**(3), 189–194 (1991).
21. A. Serov, W. Steenbergen, and F. de Mul, "Laser Doppler perfusion imaging with complementary metal oxide semiconductor image sensor," *Opt. Lett.* **27**, 300–302 (2002).
22. A. Serov, B. Steinacher, and T. Lasser, "Full-field laser Doppler perfusion imaging monitoring with an intelligent CMOS camera," *Opt. Express* **13**(10), 3681–3689 (2005).
23. K. R. Forrester, C. Stewart, J. Tulip, C. Leonard, and R. C. Bray, "Comparison of laser speckle and laser Doppler perfusion imaging, measurement in human skin and rabbit articular tissue," *Med. Biol. Eng. Comput.* **40**(6), 687–697 (2002).
24. A. Serov and T. Lasser, "High-speed laser Doppler perfusion imaging using an integrating CMOS image sensor," *Opt. Express* **13**, 6416–6428 (2005).
25. M. Atlan and M. Gross, "Laser Doppler imaging, revisited," *Rev. Sci. Instrum.* **77**, 116103 (2006).
26. M. Atlan, M. Gross, T. Vitalis, A. Rancillac, B. C. Forget, and A. K. Dunn, "Frequency-domain, wide-field laser Doppler *in vivo* imaging," *Opt. Lett.* **31**(18), 2762–2764 (2006).
27. Y. Yeh and H. Z. Cummins, "Localized fluid flow measurements with an He–Ne laser spectrometer," *Appl. Phys. Lett.* **4**, 176–179 (1964).
28. G. W. Stroke, "Lensless Fourier-transform method for optical holography," *Appl. Phys. Lett.* **6**(10), 201–203 (1965).
29. M. Gross, P. Goy, B. C. Forget, M. Atlan, F. Ramaz, A. C. Boccara, and A. K. Dunn, "Heterodyne detection of multiply scattered monochromatic light with a multipixel detector," *Opt. Lett.* **30**(11), 1357–1359 (2005).
30. M. Atlan, B. C. Forget, F. Ramaz, A. C. Boccara, and M. Gross, "Pulsed acousto-optic imaging in dynamic scattering media with heterodyne parallel speckle detection," *Opt. Lett.* **30**(11), 1360–1362 (2005).
31. M. Gross, P. Goy, and M. Al-Koussa, "Shot-noise detection of ultrasound-tagged photons in ultrasound-modulated optical imaging," *Opt. Lett.* **28**, 2482–2484 (2003).
32. F. LeClerc, L. Collot, and M. Gross, "Numerical heterodyne holography with two-dimensional photodetector arrays," *Opt. Lett.* **25**(10), 716–718 (2000).
33. U. Schnars, "Direct phase determination in hologram interferometry with use of digitally recorded holograms," *J. Opt. Soc. Am. A* **11**(7), 2011–2015 (1994).
34. C. Wagner, S. Seebacher, W. Osten, and W. Juptner, "Digital recording and numerical reconstruction of lensless Fourier holograms in optical metrology," *Appl. Opt.* **38**, 4812–4820 (1999).

35. P. Starukhin, S. Ulyanov, E. Galanzha, and V. Tuchin, "Blood-flow measurements with small number of scattering events," *Appl. Opt.* **39**, 2823–2830 (2000).
36. J. B. McMenamin and J. J. Volpe, "Doppler ultrasonography in the determination of neonatal brain death," *Ann. Neurol.* **14**(3), 302–307 (1983).
37. W. Weyler, Y. P. Hsu, and X. O. Breakefield, "Biochemistry and genetics of monoamine oxidase," *Pharmacol. Ther.* **47**(3), 391–417 (1990).
38. R. N. Kalaria and S. I. Harik, "Differential postnatal development of monoamine oxidases a and b in the blood-brain barrier of the rat," *J. Neurochem.* **49**, 1589–1594 (1987).
39. T. Vitalis, C. Fouquet, C. Alvarez, I. Seif, D. Price, P. Gaspar, and O. Cases, "Developmental expression of monoamine oxidases a and b in the central and peripheral nervous systems of the mouse," *J. Comp. Neurol.* **442**, 331–347 (2002).
40. A. L. Lopez de Pablo, M. Ajubita, M. C. F. Criado, and E. J. Marco, "MAO activity in serotonergic endings of rat major cerebral arteries," *J. Physiol. Biochem.* **60**, 23–29 (2004).
41. J. Hoper and E. Kozniewska, "Attenuation of hypoxic response in cerebral microcirculation following deprenyl," *Int. J. Microcirc.: Clin. Exp.* **11**(3), 287–295 (1992).
42. D. P. Holschneider, O. U. Scremin, L. Huynh, K. Chen, I. Seif, and J. C. Shih, "Regional cerebral cortical activation in monoamine oxidase a-deficient mice, differential effects of chronic versus acute elevations in serotonin and norepinephrine," *Neuroscience* **101**, 869–877 (2000).
43. U. Schnars and W. P. O. Juptner, "Digital recording and numerical reconstruction of holograms," *Meas. Sci. Technol.* **13**, R85–R101 (2002).
44. O. U. Scremin, *The Rat Nervous System (Cerebral Vascular System)*, 2nd ed., Academic Press, Sydney, Australia (1995).
45. A. A. Parsons, "5-ht receptors in human and animal cerebrovasculature," *Trends Pharmacol. Sci.* **12**, 310–315 (1991).
46. J. Lincoln, "Innervation of cerebral arteries by nerves containing 5-hydroxytryptamine and noradrenaline," *Pharmacol. Ther.* **68**(3), 473–501 (1995).
47. E. Hamel, J. P. Robert, A. R. Young, and E. T. MacKenzie, "Pharmacological properties of the receptor(s) involved in the 5-hydroxytryptamine-induced contraction of the feline middle cerebral artery," *J. Pharmacol. Exp. Ther.* **249**(3), 879–889 (1989).
48. T. Lee, M. Ueno, N. Sunagane, and M. Sun, "Serotonin relaxes porcine pial veins," *Am. J. Physiol.* **266**(3), H1000–H1006 (1994).
49. G. A. Lambert, C. Donaldson, K. Hoskin, P. M. Boers, and A. S. Zagami, "Dilatation induced by 5-ht in the middle meningeal artery of the anaesthetised cat," *Naunyn-Schmiedeberg's Arch. Pharmacol.* **369**(6), 591–601 (2004).
50. M. L. Cohen, K. W. Schenck, and S. H. Hemrick-Luecke, "5-hydroxytryptamine(1a) receptor activation enhance norepinephrine release from the nerve in the rabbit saphepus vein," *J. Pharmacol. Exp. Ther.* **290**, 1195–1201 (1999).
51. P. M. Vanhoutte and T. F. Luscher, "Serotonin and the blood vessel wall," *J. Hypertens. Suppl.* **4**, S29–35 (1986).